*Kufa Journal of Engineering*
*Vol. 17, No. 2, April 2026, P.P. 514-527*
*Article history: Received 17 May 2025, last revised 1 August 2025, accepted 11 August 2025*

# PERFORMANCE EVALUATION OF SUPER TWISTING SLIDING MODE CONTROL IN SWITCHED RELUCTANCE MOTOR DRIVE

**Yuser Ibrahim[1] and Abdal-Razak Shehab Hadi[2]**

**[1] Student in the Department of Electrical Engineering, University of Kufa, Najaf, Iraq, Email:yuseri.merie@student.uokufa.edu.iq.**

**[2] Professor in the department of Electrical Engineering, University of Kufa, Najaf, Iraq, Email:abdulrazzaq.aljuburi@uokufa.edu.iq.**

**https://doi.org/10.30572/2018/KJE/170231**

## ABSTRACT

Given the importance of speed control in switched-reluctance motor (SRM) drives for industrial applications, this study proposes a super-twisting sliding-mode controller (STSMC) implemented in MATLAB/Simulink to control the speed of a 6/4 SRM. Another control strategy based on speed control is implemented: conventional sliding-mode control, an optimized cascaded PID, and a traditional PID. Simulation results indicate that STSMC outperforms all other controllers, reducing speed error by 82.1% (at full load) compared to SMc and 98.2% relative to cascaded PID and PID. Regarding settling time, STSMC responds 23.1% faster than SMC (at 50 nm load) and 95% faster than Cascaded PID (at no load). Torque ripple is minimized by 47.7% and 86.7% relative to SMC and PID-based controllers, respectively. Moreover, STSMC significantly mitigates chattering in SMC, resulting in smoother control signals. These results confirm STSMC as an accurate, robust, and efficient solution for high-performance applications in SRM drives.

## KEYWORDS

Switched reluctance motor drive. 6/4 SRM. Speed control. Sliding mode control, super twisting, PID, cascaded PID, torque ripple.

## 1. INTRODUCTION

Recently, the switched-reluctance motor (SRM) has attracted significant interest among researchers due to advances in power-electronic converter technology and control algorithms. Its robust construction makes it suitable for high-speed applications, low cost, and fault-tolerant operation capability. SRM is used extensively in aerospace systems due to its lightweight design and ease of maintenance (Abdollahi et al., 2023), robotic control (Azhari *et al.*, 2024), and electric vehicles (Abdel-Aziz, Elgenedy, and Williams, 2024). The SRM introduces inherent challenges, involving nonlinear magnetic characteristics, distinct torque ripple, and elevated acoustic noise, primarily due to its doubly salient construction

configuration (Mohammed and Hadi, 2024). These factors adversely impact the overall stability and performance of the SRM drive system. Speed control is crucial to compensate for SRM non-linearities. Furthermore, SRMs often experience sudden load changes. Robust speed control ensures stable and fast speed tracking despite these disturbances. Additionally, applications such as EVs and aircraft require stable performance across a wide speed range, including low-torque, high-speed, and high-torque, low-speed conditions. This necessitates dynamic and adaptive control. Consequently, extensive research has focused on enhancing SRM performance by developing and implementing speed-control strategies. Zhang et al. (2022) proposed an approach to optimize SRM switching angles to achieve more precise speed control and smoother operation. Also, the researchers in (Jabari and Rad, 2023) optimized Cascaded PID (Proportional Integral Derivative) and Fractional Order PID (FOPID) controllers using the Dung Beetle Optimizer (DBO) and Ant-Lion Optimizer (ALO) for SRM speed regulation and torque ripple reduction. Their methodology exhibited improved dynamic speed performance and reduced ripple across various load conditions. Another control approach proposed in (Manaswi et al., 2023) is a Pulse-Width Modulation (PWM)- based speed control for an 8/6 SRM using the TMS320F28069 microcontroller, emphasizing real-time closed-loop performance. The proposed controller integrates position sensing, signal conditioning, and soft chopping techniques to enhance voltage regulation and speed accuracy. The results validated the approach's effectiveness, exhibiting smooth motor operation with reduced noise and reliable phase control. (Kotb et al., 2022) proposed a cascaded PID controller optimized by Spotted Hyena Optimizer (SHO) to enhance SRM speed control and minimize torque ripple. The SHO-based controller outperformed traditional FOPID designs in speed response, current, and torque ripple under varying load conditions. Their technique demonstrated superior convergence, robustness, and lower computational effort. However, traditional regulation methods cannot achieve accurate control, especially under load disturbances and uncertainties. The sliding-

mode controller (SMC) and model-predictive speed control (Sun et al., 2024) perform well in nonlinear systems such as SRMs and are distinguished by their simplicity and robustness to parameter variations and external disturbances. Nevertheless, the discontinuity of the control action causes chattering in conventional SMC control (Hadi, Alamili, and Kadhum, 2025). The Super-Twisting Sliding Mode Control (STSMC) for 8/6 SRM in electric vehicle (EV) drivetrains is proposed in (Sehab, Akrad, and Saadi, 2023) to prevent the chattering in the control signal. The simulation results demonstrate the robustness of (STSMC) against model uncertainties, minimize torque ripples, and improve speed-tracking accuracy compared to PI and Conventional Sliding Mode Control (CSMC). (Zhang et al., 2025) proposed an improved speed control strategy for 12/8 SRM by integrating Super-Twisting Sliding Mode Control (STSM) with Linear Active Disturbance Rejection Control (LADRC). The method improves dynamic response and disturbance rejection by optimizing the observer and replacing discontinuous functions with smooth sigmoid functions. Results show superior performance over conventional Proportional-Integral PI and STSM in reducing settling time and torque ripple. In contrast (Robson Costa et al., 2025) proposed a novel Linear-Quadratic-Integral (LQI) speed controller for 12/8 SRM, eliminating the need for an inner current loop. The proposed controller demonstrated improved disturbance rejection and a fixed switching frequency compared with traditional PI and Hysteresis controllers. The results validated the LQI's superior performance across changes in speed, load, and supply conditions. Moreover, (Soliman, Ahmed, and Sharaf) presented a fuzzy logic-based control strategy to enhance speed regulation and reduce torque ripples for SRMs. The proposed method achieves faster speed convergence across varying load conditions and reduces torque ripple by 65–75% compared with conventional PI controllers. This paper focuses on the design and comparison of Super-Twisting SMC (STSMC), conventional Sliding Mode Control (SMC), PID, and cascaded PID for SRM speed control under parameter variations and load disturbances. It evaluates their performance in speed tracking, settling time, torque ripple reduction, and robustness. The ultimate goal is to demonstrate that STSMC achieves superior performance compared with all conventional controllers used in this study.

## 2. MODELLING OF SRM DRIVE

SRM is a nonlinear system motor with six and four salient poles on both the stator and the rotor, respectively, with windings placed around the stator only; these windings couple opposed pairs to represent the motor phases as shown in Fig. 1 (Bilgin, Jiang, and Emadi, 2019). The excitation circuit consists of an Asymmetric Half-Bridge (AHB) converter. The rotor rotates as the excitation alternates between phases. The principle of operation of SRM is based on

generating electromagnetic torque by varying magnetic reluctance, which depends on rotor position and is associated with each excited phase. The SRM parameters are shown in Table1 .

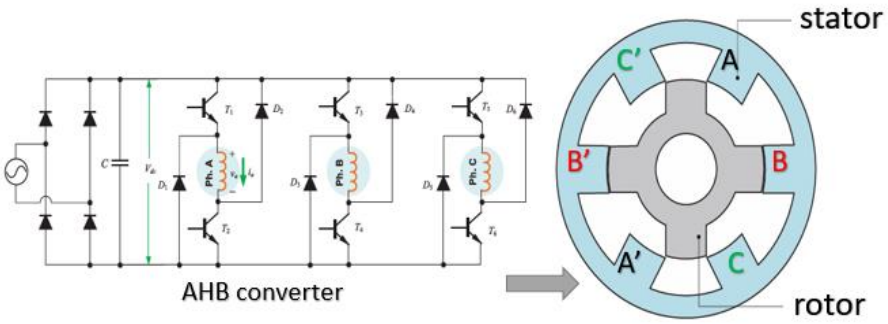


**Fig.1. Cross-section view of 6/4 SRM with excitation circuit**

The mathematical model of SRM consists of several electrical and mechanical system equations. The voltage equation for SRM:

$$u = Ri + \frac{d\psi(i,\theta)}{dt}$$ (Sun *et al.*, 2024; Bilgin, Jiang and Emadi, 2019) (1)

Where R is the resistance per phase, and ψ is the flux linkage per phase, the flux linkage per phase given by:

$$\psi(i,\theta) = L(i,\theta)i \quad (2)$$

Where $L(i,\theta)$ is the phase inductance, it is a nonlinear function of the phase current $(i)$ and rotor position $(\theta)$. By differentiating Eq.1 with respect to the rotor position (θ) and the phase current $(i)$, the following equation is achieved :(Bilgin, Jiang, and Emadi, 2019)

$$u = Ri + \frac{d\psi(i,\theta)}{d\theta}.\frac{d\theta}{dt} + \frac{d\psi(i,\theta)}{di}.\frac{di}{dt} \quad (3)$$

Where $\frac{d\theta}{dt} = \omega$ and $\omega$ is the actual motor speed in rad/s, and $(u)$ represents voltage per phase. Rearranging Eq.3 will produce the following equation :

$$\frac{di}{dt} = (u - Ri - \omega \frac{d\psi(i,\theta)}{d\theta})(\frac{d\psi(i,\theta)}{di})^{-1}$$ (Bilgin, Jiang and Emadi, 2019) (4)

The dynamic equations of SRM :

$$\dot{\omega} = \frac{1}{J}(T - T_L - B\,\omega)$$ (Bilgin, Jiang and Emadi, 2019) (5)

Where:

$T$ = total electromagnetic torque (N· m)

$T_L$= load torque (N.m)

B = friction coefficient (N.m.s)

J= moment of inertia (kg.$m^2$).

ω = motor speed (rad/s)

The torque equivalent $(T)$ equals the summation of torques produced by each phase. For m-

phases, the equivalent torque is given by (Bilgin, Jiang, and Emadi, 2019) :

$$T = \sum_{j=1}^{m} T_j \quad (6)$$

Where $T_j$ is the torque per phase.

$$T_j = \frac{1}{2} i^2 \frac{dL}{d\theta} \quad \text{(Bilgin, Jiang and Emadi, 2019)} \quad (7)$$

**Table 1. Parameters of the 6/4 Switched Reluctance Motor (SRM) Drive System.**

| No. | Parameter | Symbol |
|---|---|---|
| 1 | Motor type | 6/4 |
| 2 | Number of phases (m) | 3 |
| 3 | Rated power | 60 kw |
| 4 | Resistance per phase ($R$) | 0.02 Ω |
| 5 | Moment of inertia (J) | 0.02 kg.$m^2$ |
| 6 | friction coefficient (B) | 0.05 N · m · s |
| 7 | Nominal speed | 3000 r.p.m |
| 8 | full load torque (TL) | 100 N.m |
| 9 | Maximum current | 450 A |
| 10 | DC supply voltage (Vdc) | 240 V |

## 3. CONTROL STRATEGIES FOR SRM

### 3.1. PID control

A PID (proportional- integral- derivative) controller regulates the speed output based on the speed error using three terms: proportional, integral, and derivative. It is widely used in system engineering systems for its simplicity. The Speed error for SRM

$$e_\omega(t) = \omega - \omega d \quad (8)$$

where $e_\omega(t)$ equals the difference between actual and reference speeds. The PID control law for the SRM speed loop is:

$$u(t) = Kpe_\omega(t) + Ki \int_0^t e_\omega(\tau)d\tau + Kd\, \dot{e_\omega} \quad (9)$$

$Kp$, $Ki$, and $Kd$ are proportional, integral, and derivative positive controller constants, respectively.

### 3.2. Cascaded PID Control

The Cascaded PID with spotted hyena optimization algorithm-based speed control method (Kotb et al., 2022) was re-implemented under similar parameters and conditions to compare its performance with that of the proposed method. The Cascaded PID structure was designed with:

- Outer loop for speed control. The speed tracking error equals the difference between the actual and reference speeds, as in (8). The outer PID1( $u_1(t)$ ) produced a reference current ($i_{ref}$) (Kotb *et al.*, 2022):

$$u_1(t) = i_{ref} = Kp_1 e_\omega(t) + Ki_1 \int_0^t e_\omega(\tau)d\tau + Kd_1 \frac{de_\omega(t)}{dt} \quad (10)$$

- Inner loop for current control

$$\text{current error } e_i(t) = i_{ref} - i_{act} \quad (11)$$

$i_{act}$= actual motor current in (A)

The inner PID2 control law $u_2(t)$ (Kotb *et al.*, 2022)

$$u_2(t)=Kp_2 e_i(t) + Ki_2 \int_0^t e_i(\tau)d\tau + Kd_2 \frac{de_i(t)}{dt} \quad (12)$$

Where $Kp_1$,$Ki_1$, $Kd_1$,$Kp_1$, $Ki_2$, $Kd_2$ are positive constant controllers.

### 3.3. Sliding Mode Control (SMC)

A variable-structure controller adapts its structure to the system's current state and drives the system to track the sliding surface s(t). The conventional SMC sliding surface for the nonlinear second-order system based on the tracking system's error e(t) in (8) takes the following form:

$$S(t)= \dot{e}+ \lambda e \quad \text{(Hou, Fang and Lien, 2017)} \quad (13)$$

The control law u(t) that compels the system trajectories to the sliding surface consists of two parts (Hou, Fang and Lien, 2017) :

$$u(t)=u_{eq}+u_{sw} \quad (14)$$

Where the part $u_{eq}$is the equivalent control law, which can be defined as the continuous control law that would maintain $\dot{s}(t)$=0, and $u_{sw}$ is the corrective term which compensates the variations of the state's trajectories from the time-varying sliding surface $s\ (t)$ to reach it. By differentiating equation (5) as follows:

$$\ddot{\omega}=\frac{1}{J}\frac{\partial T}{\partial i}\left(\frac{\partial \psi}{\partial i}\right)^{-1}\left(-Ri- \omega \frac{\partial \psi}{\partial \theta}\right)+\frac{1}{J}\left(\frac{\partial T}{\partial \theta}\omega - \dot{T}L - B\dot{\omega}\right)+\frac{1}{J}\frac{\partial T}{\partial i}\left(\frac{\partial \psi}{\partial i}\right)^{-1} u(t) \quad (15)$$

Which can be written in the form :

$$\ddot{\omega}=f(\omega, \theta, i, \psi, \dot{\omega}, T, R, \dot{T}L, B)+g(\theta, i)\, u(t) \quad (16)$$

u(t) represents the input of m phase voltages, and the functions (f) and (g) represent the dynamic system's behavioral and control input effects, respectively. The equivalent SMC control law for the SRM system

$$u_{eq}(t)=\frac{1}{g(\theta,i)}[\ \ddot{\omega}d - f(\omega, \theta, i, \psi, \dot{\omega}, T, R, \dot{T}L, B) - \lambda\dot{e}] \quad (17)$$

The corrective term $u_{sw}$of the SMC control law is found using the Lyapunov function:

$$V=\frac{1}{2}S^2 \quad (18)$$

The $\dot{V}(S)$ must be a negative value to satisfy the stabilité conditions of the controlled system

$$\dot{V}(S)=S\dot{S}<0 \quad (19)$$

A reaching law $(u_{eq})$is used to obtain the correction law :

$$u_{sw}=Ksgn(s) \quad (20)$$

Where k > 0 is the design constant to control the appropriate uncertainties, and sgn(s) denotes the sign function. This function in the control law leads to chattering (high-frequency oscillations). The complete equation of the SMC control law for the SRM system has the following form :

$$u(t)=\frac{1}{g(\theta,i)}[\ \ddot{\omega}d\text{-f}(\omega,\theta,i,\psi,\dot{\omega},T,R,\dot{T}L,\text{B})\text{-}\lambda\dot{e}-\text{Ksgn(s)}] \quad (21)$$

### 3.4. Super Twisting Sliding Mode Control (STSMC)

Unlike conventional SMC, which exhibits high-frequency switching (chattering), the Super-Twisting Algorithm (STA) yields a continuous second-order sliding mode (SOSM), as shown in Fig. 4. It exhibits super-twisting convergence in the (s) plane (Mohapatra et al., 2024), thereby eliminating chattering while maintaining robustness. The sliding variable s(t) is based on the Tracking error in (8) :

$$\text{s(t)}=\dot{e}+\lambda_1 e \quad (22)$$

where $\lambda_1 > 0$ is a positive constant determining the error convergence rate. The STSMC control law is defined as (Mohapatra *et al.*, 2024):

$$\text{u(t)}=u_1(t)+u_2(t) \quad (23)$$

$$u_1(t)=\begin{cases}-\mu\,|s_o|^{\rho}\text{sign(s)} & \text{if } |\text{u}|>s_o\\ -\mu\,|s_o|^{\rho}\text{sign(s)} & \text{if not}\end{cases} \text{ (Mohapatra } et\ al.\text{, 2024)} \quad (24)$$

$$\dot{u2}(\text{t})=\begin{cases}-\text{u} & \text{if}|\text{u}|>\text{UM}\\ -\alpha\text{sign(s)} & \text{if not}\end{cases} \quad (25)$$

With constants ρ, μ, and α, checking for the following conditions (Mohapatra et al., 2024):

$$\begin{cases}\alpha > C_O/\text{Km} & ,\ 0<\rho<0.5\\ \mu^2=4\,C_O\,\text{KM}\,(\alpha+C_O)/\,Km^2\text{Km}(\alpha-C_O)\end{cases} \quad (26)$$

Where KM, Km, and $C_O$ are positive constant coefficients. Make $s_o=\infty$ for a simple process (Mohapatra *et al.*, 2024).

$$\begin{cases}u_1(t)=-\mu|\text{s}|^{\rho}\text{sign(s)}+u2(\text{t})\\ \dot{u2}(\text{t})=-\alpha\ \text{sign(s)}\end{cases} \quad (27)$$

The proposed control STSMC scheme is shown in Fig. 2. It consists of two control loops. The outer speed loop governs motor speed by generating a reference torque based on the speed error, and the inner torque loop generates the actual electromagnetic torque to match the torque demand. Torque demand is translated into phase-current references required to produce the desired torque, as shown in Eq.7 A Pulse Width Modulation (PWM) converts the reference torque into gating signals for the Asymmetric Half Bridge converter (AHB). The converter excites the SRM stator windings at the appropriate turn-on and turn-off angles, as determined by the rotor position sensor. Fig. 4 shows the block diagram of the proposed controller. The

block (f) represents Eq.15, the block (g) represents Eq.16, and the block(w) represents Eq.30. The controller output equals the reference torque. Each cascaded PID controller (Kotb et al., 2022), the PID controller, the conventional SMC, and the proposed STSMC were tested on the same 6/4 SRM model in MATLAB/SIMULINK, using identical system parameters as in Table1. The same speed profile changes and load torque disturbances were applied to ensure similar testing conditions. All controller parameters, except the cascaded PID controller, were tuned individually via trial-and-error to achieve optimal performance under identical conditions. Table 2 summarizes the final parameters for the proposed STSMC, classical SMC, Cascaded PID, and the traditional PID controller.

**Table 2. Parameters of the control schemes**

| No. | Controller | Parameters |
|---|---|---|
| 1 | STSMC | $\lambda_1 = 90, \mu = 4, \rho = 0.5, \alpha = 50.$ |
| 2 | SMC | $\lambda$=100 ,K=300 |
| 3 | Cascaded PID | $Kp_1$=12.2799,$Ki_1 = 10.89, Kd_1$=0, =18.6819,$Ki_2 = 20, Kd_2$=18.7407 (Kotb et al., 2022) |
| 4 | PID | $K_p$= 15, $K_i = 1$, $K_d$=3 |
| 5 | Turn on and turn off angles. | $\theta_{on}$=45°,$\theta_{off}$=75° |

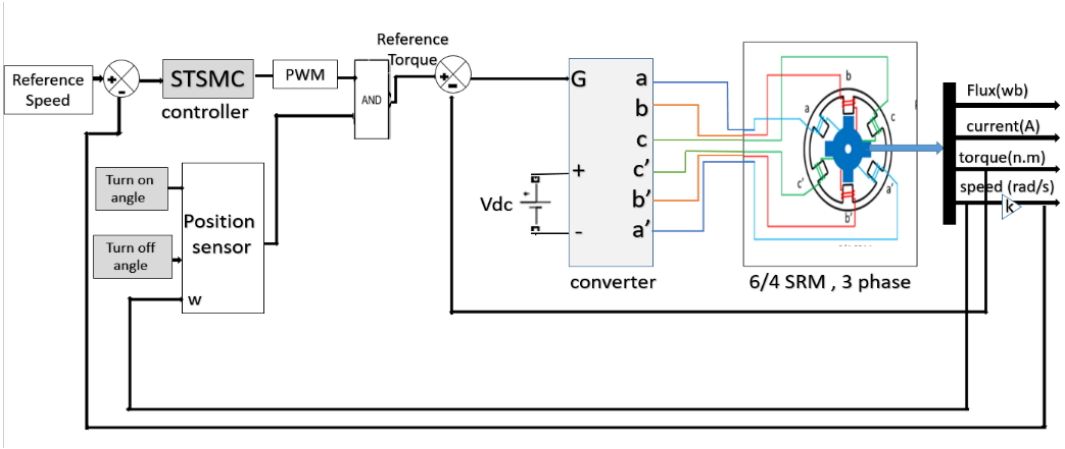


**Fig. 2. Block diagram of SRM with proposed controller.**

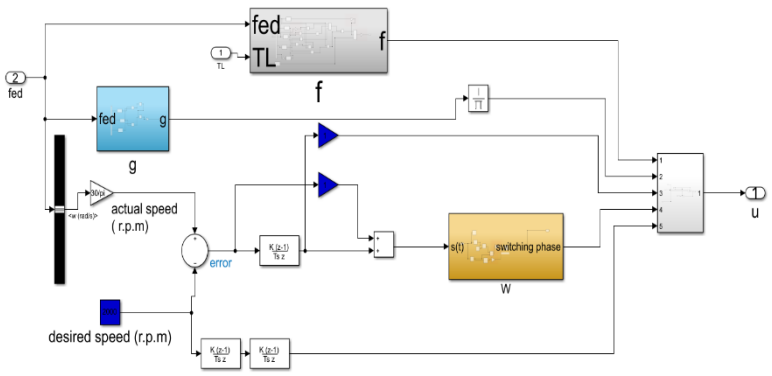


**Fig. 3. The proposed STSMC controller**

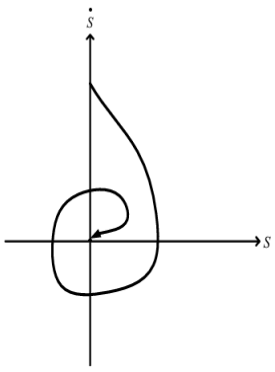


**Fig.4. super twisting convergence in (s) plane**

## 4. RESULTS AND DISCUSSION

### 4.1. Static load

With a desired speed of 3000 rpm, STSMC across all load conditions (no load, 50 N·m, and 100 N·m) achieves the fastest settling time (0.1–0.17 s), as shown in Figs. 5a, 5b, 5c, and Table 3, while PID and Cascaded PID (Kotb *et al.*, 2022) exhibit much slower dynamics (up to 3.1 s). Overshoot is almost eliminated in STSMC (0.16%) and SMC (0.3%) at no load Fig. 5a, whereas PID shows noticeable overshoot (up to 6% at no load). Steady-state speed error remains minimal for STSMC (0.5 rpm at no load, 3 rpm at 50 N·m, and 9 rpm at 100 N·m), while SMC increases to 11 rpm, 50 rpm at 50 N ·m, and 100 N·m, respectively, and PID-based controllers in Fig. 5c. degrade up to 500 rpm under heavy load. Due to their fixed gains, lack of disturbance rejection, and slow integral response, they are unsuitable for high-nonlinear SRM dynamics. Torque ripple Figs. 5.d, e, f is significantly minimized by STSMC (0.35–0.38%), slightly better than SMC (0.4–0.67%), and far superior to Cascaded PID and PID (>2%). Even under the full load of 100 N·m, STSMC maintains smooth torque and accurate speed tracking. Another Previous study on fuzzy logic controllers (Soliman, Ahmed and Sharaf, 2025) for SRM speed control has limitations, such as slower dynamic response. The proposed STSMC improves performance, achieving a 78.5% reduction in settling time relative to the previous study. These results from Fig. 5 and Table 3 confirm STSMC's superior robustness, fast response, and torque ripple suppression due to STSMC's robust nonlinear structure and second-order sliding mode (SOSM) mechanism, which provides fast convergence.

### 4.2. Chattering

Fig.6. describes the qualitative difference in control behaviour between the SMC and STSMC strategies. The conventional SMC control law results in high-frequency switching and sharp chattering, as evidenced by the square-wave control signal. In contrast, the STSMC control law produces a continuous, progressively varying control signal that eliminates chattering while preserving robustness. This smooth control effort improves energy efficiency and practical applicability of the SRM system under real-time operating conditions.

### 4.3. Load torque changes

Here, the SRM operated at a speed reference of 3000 rpm. A variable load profile was applied, starting at no load (0 s). A 50 N·m load was applied at 2.5 s, followed by a 100 N·m load at 3.5 s, causing only a < 10 rpm fall after 3.5s for the proposed STSMC with a fast settling time of about 0.1s as in Fig. 7. The SMC showed a higher deviation of nearly 30 rpm when the load reached 100 N·m (at 3.5 s). In comparison, PID dropped to above 600 rpm, and Cascaded PID to around 500 rpm. The speed drop in PID and Cascaded PID (Kotb et al., 2022) is due to their

limited disturbance rejection and slow dynamic response, as they rely on fixed linear gains that cannot accommodate SRM nonlinearities. This prevents them from maintaining the 3000 rpm reference under sudden load changes, resulting in the largest deviations and the longest recovery times. These approximate results confirm STSMC's superior robustness and its fastest response to load disturbances.

### 4.4. Sudden speed changes

Fig. 8 shows that at 0 s, the reference speed was set to 3000 rpm; STSMC reached it rapidly, SMC was slightly slower, whereas Cascaded PID and PID lagged significantly. At 2 s, the reference increased to 4000 rpm; STSMC tracked instantaneously with negligible tracking error, SMC showed about 50 rpm lag, while PID-based controllers had significant speed errors. At 3.5 s, the reference dropped to 2000 rpm; STSMC followed smoothly, SMC settled more slowly, and PID/Cascaded PID showed undershoot and prolonged recovery. Cascaded PID shows high-speed ripple at steady state (after 9 s), while PID and SMC maintain small ripples. Across all transitions, STSMC had the fastest response time and the highest accuracy.

### 4.5. Unknown disturbances

Under a 50 Hz, 20,000-amplitude random disturbance, the proposed STSMC maintained the desired output with superior disturbance rejection, as demonstrated in Fig. 9. The SMC showed good robustness. Cascaded PID diverged completely due to integral windup, proving the least robust under random disturbances. PID exhibited small oscillations near zero speed as it lacks adaptability to high-frequency noise.

**Table 3. Comparative performance for all controllers under different load torques.**

| Controller | Load (N.m) | Settling time (s) | Overshoot (%) | Steady state Error in r.p.m | Torque Ripple (%) |
|---|---|---|---|---|---|
| STSMC | No load | 0.1 | 0.16 | 0.5 | 0.38 |
| | 50 | 0.13 | 0 | 3 | 0.37 |
| | 100 | 0.17 | 0 | 9 | 0.35 |
| SMC | No load | 0.15 | 0.3 | 2 | 0.4 |
| | 50 | 0.17 | 0 | 11 | 0.65 |
| | 100 | 0.20 | 0 | 50 | 0.67 |
| Cascaded PID | No load | 2 | 2 | 5 | 2.9 |
| | 50 | 0.45 | 0 | 60 | 0.90 |
| | 100 | 0.25 | 0 | 500 | 2.6 |
| PID | No load | 3.1 | 6 | 4 | 0.64 |
| | 50 | 0.6 | 0 | 65 | 0.91 |
| | 100 | 0.64 | 0 | 500 | 2.6 |

## 5. CONCLUSION

This study conducted an inclusive comparative analysis of four control strategies: STSMC, SMC, Cascaded PID, and PID for the speed regulation of SRM under varying speeds and load torques. The results demonstrated the superiority of the proposed STSMC across all operating

conditions. STSMC exhibited improved performance, with a 23.1% shorter settling time, 47.0% lower overshoot, 80.1% lower speed error, 47.7% lower torque ripple, and lower chattering than the more robust SMC. Compared to the optimized Cascaded PID controller, the STSMC demonstrated significant improvements of 85.2%, 92%, 98.8% (at full load), and 86.5% in the same metrics. Compared to the conventional PID controller, STSMC achieved a 96.8% reduction in settling time and a 94.8% reduction in overshoot. However, STSMC has limitations, including sensitivity to parameter tuning and dependence on accurate system modelling. To address these challenges, future work will integrate intelligent optimization methods (e.g., PSO or MODA), evolve adaptive or neural-network-based STSMC structures for online tuning, and implement real-time control on embedded systems.

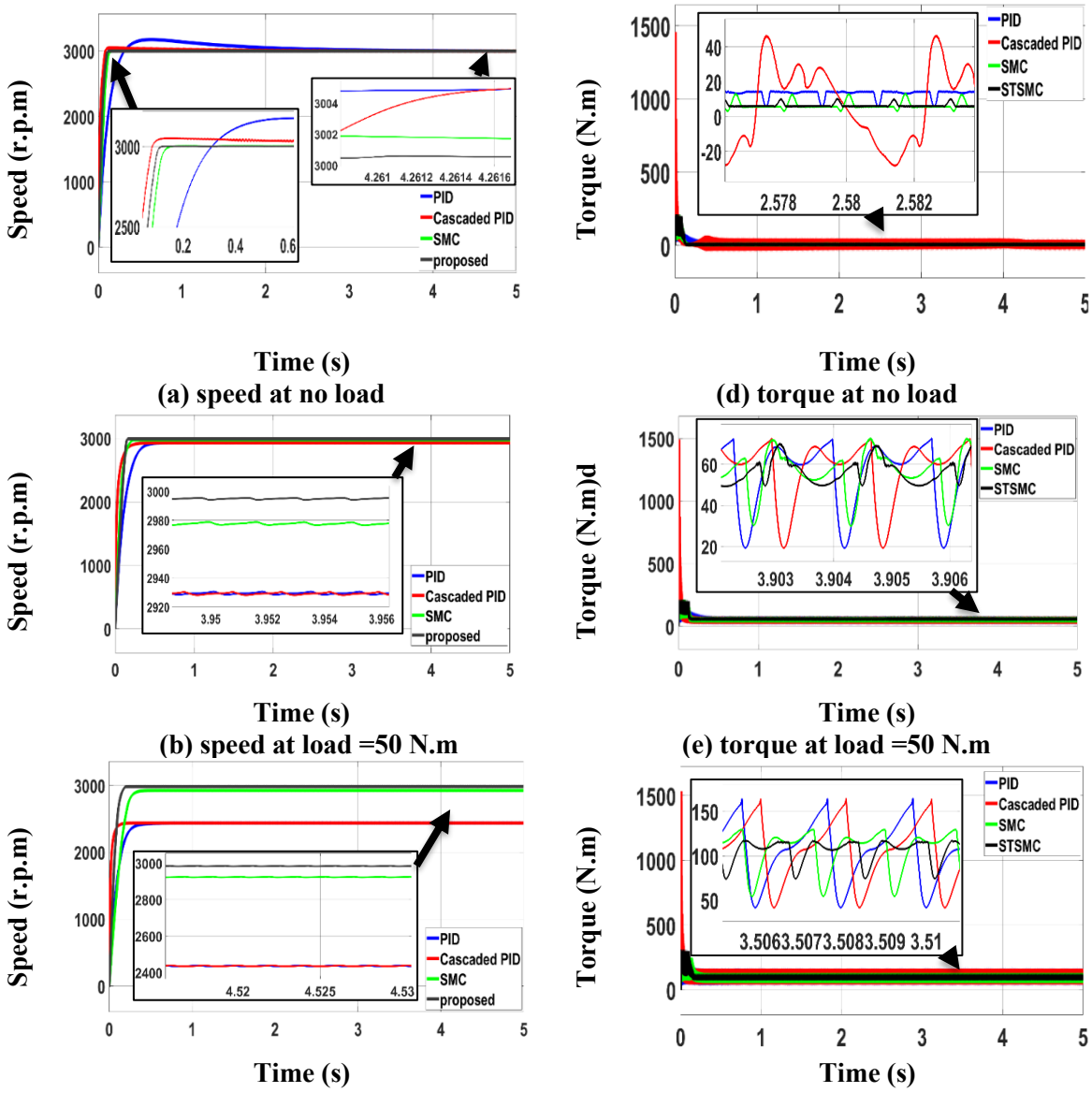


(a) speed at no load (d) torque at no load

(b) speed at load =50 N.m (e) torque at load =50 N.m

(c) speed at load =100 N.m (f) torque at load =100 N.m

**Fig.5. speed and torque responses for all controllers under variable load torque conditions**

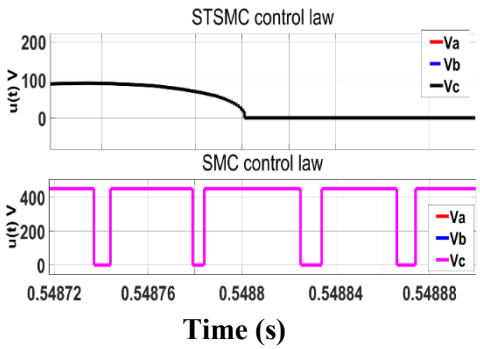


**Fig.6.control law for SMC and STSMC**

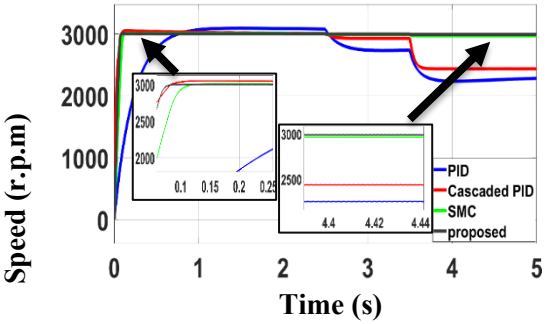


**Fig.7.speed response for all controller under dynamic load case**

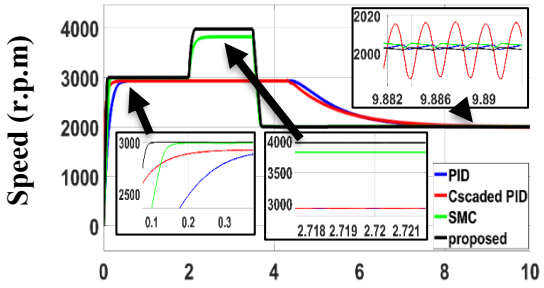


**Fig.8.speed tracking for all controller under speed changes**

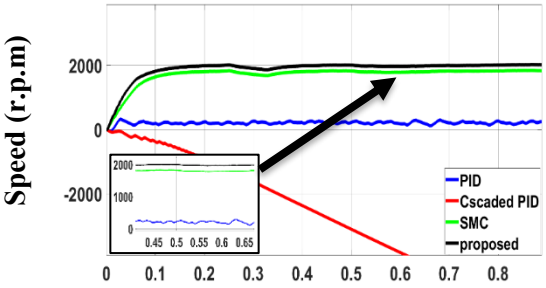


**Fig.9.speed tracking for all controller under unknown disturbance**

## 6. REFERENCES

Abdel-Aziz, A., Elgenedy, M. and Williams, B. (2024) 'Review of Switched Reluctance Motor Converters and Torque Ripple Minimisation Techniques for Electric Vehicle Applications', Energies , 17(13). Available at: https://doi.org/10.3390/en17133263.

Abdollahi, M.E. et al. (2023) 'Switched Reluctance Motor Design for a Light Sport Aircraft Application', Machines, 11(3). Available at: https://doi.org/10.3390/machines11030362.

Azhari, B. et al. (2024) 'Design of switched reluctance motor as actuator in an end-effector-based wrist rehabilitation robot', Journal of Mechatronics, Electrical Power, and Vehicular Technology, 15(2), pp. 220–229. Available at: https://doi.org/10.55981/j.mev.2024.1109.

Bilgin, B., Jiang, J.W. and Emadi, A. (2019) Switched Reluctance Motor Drives Fundamentals to Applications, CRC Press, Tylor and Francis Group.

Hadi, A.R.S., Alamili, A. and Kadhum, A.A. (2025) 'Robust Sliding-Mode-Based Learning for Maximum Power Point Tracking Photovoltaics System', Kufa Journal of Engineering, 16(2), pp. 249–262. Available at: https://doi.org/10.30572/2018/KJE/160215.

Hou, Y.-Y., Fang, C.-S. and Lien, C.-H. (2017) 'Sliding Mode Control Design for Some Classes of Chaotic Systems BT - Applications of Sliding Mode Control in Science and Engineering',

in S. Vaidyanathan and C.-H. Lien (eds). Cham: Springer International Publishing, pp. 1–33. Available at: https://doi.org/10.1007/978-3-319-55598-0_1.

Jabari, M. and Rad, A. (no date) 'Optimization of Speed Control and Reduction of Torque Ripple in Switched Reluctance Motors Using Metaheuristic Algorithms Based PID and FOPID Controllers at the Edge'. Available at: https://doi.org/10.26599/TST.2024.9010021.

Kotb, H. et al. (2022) 'Speed control and torque ripple minimization of SRM using local unimodal sampling and spotted hyena algorithms based cascaded PID controller', Ain Shams Engineering Journal, 13(4). Available at: https://doi.org/10.1016/j.asej.2022.101719.

Manaswi, K. et al. (2023) 'Implementation of PWM Speed control for SRM drive using TMS320F28069 Microcontroller', Proceedings of the 2023 1st International Conference on Cyber Physical Systems, Power Electronics and Electric Vehicles, ICPEEV 2023, pp. 1–6. Available at: https://doi.org/10.1109/ICPEEV58650.2023.10391895.

Mohammed, Z.R. and Hadi, A.R.S. (2024) 'Torque Ripple Rate Reduction of 6/4 Switched Reluctance Motor Using Sliding Mode Learning Controls', Kufa Journal of Engineering, 15(4), pp. 18–33. Available at: https://doi.org/10.30572/2018/KJE/150402.

Mohapatra, B. et al. (2024) 'Optimizing grid-connected PV systems with novel super-twisting sliding mode controllers for real-time power management', Scientific Reports, 14(1), pp. 1–22. Available at: https://doi.org/10.1038/s41598-024-55380-3.

Robson Costa, P.M. et al. (2025) 'A Novel LQI-Based Speed Control of Switched Reluctance Motors for High Performance Applications', IEEE Access, 13, pp. 7437–7447. Available at: https://doi.org/10.1109/ACCESS.2025.3525553.

Sehab, R., Akrad, A. and Saadi, Y. (2023) 'Super-Twisting Sliding Mode Control to Improve Performances and Robustness of a Switched Reluctance Machine for an Electric Vehicle Drivetrain Application †', Energies, 16(7). Available at: https://doi.org/10.3390/en16073212.

Soliman, R.F., Ahmed, M.R. and Sharaf, S.M. (2025) 'Torque ripples reduction and speed control of a switched reluctance motor based on artificial intelligence techniques', International Journal of Power Electronics and Drive Systems, 16(2), pp. 936–948. Available at: https://doi.org/10.11591/ijpeds.v16.i2.pp936-948.

Sun, X. et al. (2024) Multi-objective Design Optimization of Switched Reluctance Motor Drive Systems, Multi-objective Design Optimization of Switched Reluctance Motor Drive Systems. Available at: https://doi.org/10.1007/978-981-96-0672-6.

Zhang, J. et al. (2025) 'Research on Speed Control of Switched Reluctance Motors Based on Improved Super-Twisting Sliding Mode and Linear Active Disturbance Rejection Control', Electronics (Switzerland), 14(6). Available at: https://doi.org/10.3390/electronics14061065.